Ion-beam-induced damage in silicon studied using variable-energy positrons, Rutherford backscattering, and infrared absorption

P. J. Simpson, M. Vos, I. V. Mitchell, C. Wu, and P. J. Schultz
Department of Physics, The University of Western Ontario, London, Ontario, Canada N6A 3K7
(Received 26 April 1991; revised manuscript received 15 July 1991)

Silicon (100) wafers have been irradiated at 300 K with silicon ions or helium ions at energies between 0.2 and 5.0 MeV. Fluences ranged from 10^{11} to 10^{16} cm^{-2}. The associated defect profiles have been analyzed using variable-energy positron-beam methods. Displaced-atom distributions have been extracted from Rutherford-backscattering-channeling (RBSC) measurements and supplemented by infrared (1.8 μm) absorption measurements to yield divacancy concentrations. Defect annealing is observed through the divacancy anneal stage ($\sim$470 to 570 K), He-irradiated silicon returning to single-crystal quality as measured by infrared and positron methods. For the same anneal, Si-irradiated silicon shows partial restoration of crystallinity (RBSC), no change in positron-trapping characteristics, and removal of the optically active divacancies. Annealing to between 870 and 970 K restores the crystal to near preimplant characteristics.

I. INTRODUCTION

Since the earliest reports of experiments on ion implantation into silicon,[1] a continuing interest has been shown in microscopic descriptions of the associated radiation damage. The general concepts involved in the evolution of defect structure are well known. The kinetic energy of the incoming ion is dissipated to electronic excitation and to atomic ("elastic" or "nuclear") collisions. The latter are responsible for the individual atomic displacements and displacement sequences (cascades) that produce point defects and defect ensembles, respectively, in the silicon lattice. At high deposited energy densities, of the order of 1 eV per atom, cascades may be large enough to produce lattice collapse over dimensions that are readily visible to transmission electron microscopy.[2] At the other extreme (electron, proton, and helium-ion irradiation), defect production is dominated by the generation of Frenkel pairs, with a high probability for recombination or diffusional loss of the interstitials and vacancies. To some extent the experimenter has control over the type, configuration, and number of postirradiation defects through the choice of sample temperature, of impurity type and concentration in the sample, and of the implanted ion type, energy, fluence, and flux.[3,4]

Of the many point defects identified in ion-implanted silicon,[5] the divacancy has been singled out for particular attention. In an infrared absorption study of 400-keV ^{11}B-, ^{64}Zn-, and ^{121}Sb-implanted silicon, Stein *et al.*[6] were able to relate divacancy formation to the energy deposited in collisional processes up to a critical energy density at which amorphous zones are believed to form. In their study of ion-beam-induced transitions between amorphous and crystalline phases at the crystalline-amorphous boundary in silicon, Elliman, Linnros, and Brown[3] identified the divacancy as the active defect responsible for crystal growth or amorphization, the outcome being controlled by sample temperature and ion flux. Likewise, divacancy production was identified as the central process in two discrete modes of damage accumulation during silicon self-ion irradiation.[7]

The present study has been motivated by recent developments in slow-positron-beam methods.[8] Thermalized positrons have a high probability for capture and annihilation in open volume (i.e., vacancy-type) defects. With the advent of variable-energy positron beams, the probing depth may be varied and hence the vacancy-type defect distribution derived.[9] The intent of this study was to reexamine the nature and growth of ion-beam damage in silicon using the positron-beam technique, supplemented by ion backscattering and optical absorption data. Beams of $\sim$MeV energy He and Si have been used for the irradiations to produce an abundance of relatively simple defects. Preliminary results of positron and Rutherford-backscattering-channeling (RBSC) studies of Si-implanted samples have been published elsewhere.[10]

II. EXPERIMENT

A. Implantation

Wafers of (100) *p*-type float-zone silicon 0.5 mm thick were implanted at an off-normal orientation, using the University of Western Ontario 1.7-MV Tandetron accelerator. ^{4}He ions were implanted at energies of 0.25, 0.5, 0.7, and 4 MeV, in doses from 10^{13} to 10^{16} ions cm^{-2}, and ^{28}Si ions were implanted at energies of 0.54, 3, and 5 MeV in doses from 10^{11} to 10^{15} ions cm^{-2}. The beam was rastered to give uniform irradiation over an area $\sim$75 mm in diameter. Beam current was maintained at 0.3 μA or less to minimize beam heating of the samples, although some beam heating (a few tens of degrees) did occur.[11] The samples were characterized by positron annihilation, RBSC, and infrared absorption both as implanted and after annealing stages.

B. Analytical methods

1. Positron annihilation spectroscopy

The University of Western Ontario slow-positron-beam facility is described in detail elsewhere.[12] Monoenergetic positrons (in the energy range 0.3–60 keV) are implanted into the sample. In penetrating the solid the positrons lose energy rapidly, thermalizing in ~ 10 ps. The mean depth $\bar{z}$ (Å) of implantation into the sample may be varied by changing the incident beam energy E (keV):

$$\bar{z}=(400/\rho)E^n , \tag{1}$$

where ρ is the density of the solid (g cm^{-3}) and n is a constant deduced empirically to be $n=1.6\pm0.1$.[13] The depth distribution of thermalized positrons is broad and asymmetric. It can be described by a Makhovian distribution:

$$P(z)=(mz^{m-1}/z_0^m)\exp[-(z/z_0)^m] , \tag{2}$$

with

$$z_0=\bar{z}/\Gamma[(1/m)+1] , \tag{3}$$

where $m=2.0$.[13]

The depth at which the positrons annihilate is not only determined by this broad implantation profile but also by the diffusion that occurs after the positron has thermalized. The diffusion coefficient for positrons in Si wafers at room temperature is 2.1–2.7 cm^2 s^{-1};[14] in this study we have used the value 2.1 cm^2 s^{-1}. Thermal positrons diffuse through a defect-free solid for ~ 200 ps before annihilating. In the presence of defects the number of freely diffusing positrons decreases at a rate λ_{eff}:

$$\lambda_{\text{eff}}=\lambda_f+\nu C , \tag{4}$$

where λ_f is the annihilation rate for positrons diffusing freely in the bulk solid [4.55×10^9 s^{-1} for Si [Ref. (15)], ν the trapping rate of the defects (s^{-1}) and C the defect concentration (per atom). The trapping rate ν used here is 6×10^{14} s^{-1} per defect.[15] Using this value one can calculate that 5% of the positrons will be trapped by defects at a homogeneous defect concentration of 4.0×10^{-7} per atom and 95% at a defect concentration of 1.5×10^{-4} per atom. These values determine roughly the range over which one can measure defect concentrations: Defect concentrations smaller than 4.0×10^{-7} will not trap a measurable fraction of positrons, while an increase of the defect concentration above 1.5×10^{-4} will not lead to a noticeable increase in the fraction of positrons trapped.

The surface of the solid is also an efficient trap for positrons. The positron can be reemitted from a clean surface, either free or bound with an electron as positronium, but the probability of this is negligible for the (oxide-covered) surface of samples in this study.[8]

Annihilation may thus occur from one of three possible states: freely diffusing, trapped at the surface of the solid, or trapped by a point defect. In the annihilation event, the momentum of the electron creates a Doppler shift in the energy of the γ radiation emitted. Thus the width of the 511-keV line is sensitive to the electronic environment in the solid and will differ between positrons trapped by defects and those annihilating in the perfect crystal.

In the present work, γ-ray spectra are collected with an intrinsic Ge detector of ~ 210-cm^3 volume and 1.3-keV resolution (at 511 keV), and are analyzed using the W parameter, defined as the number of counts in the wings of the 511-keV peak (507.3–509.7 and 512.3–514.7 keV) divided by the total counts in the peak (506.2–515.8 keV).

The W parameter versus energy data are analyzed using the program POSTRAP4,[16] which solves the diffusion equation for positrons in a semiconductor, including the effect of defects and electric fields. POSTRAP4 calculates, for each incident positron beam energy E, the fractions of positrons which annihilate in defects $F_d(E)$, which annihilate while freely diffusing in the bulk crystal $F_f(E)$, and which annihilate at the surface $F_s(E)$, for each model of defects and electric fields in the sample. The experimental line-shape parameter $W(E)$ can then be fitted using the equation

$$W(E)=W_sF_s(E)+W_fF_f(E)+W_dF_d(E) , \tag{5}$$

where W_s, W_f, and W_d are the characteristic line-shape parameters for annihilation at the surface, freely diffusing in the bulk, and trapped in a defect, respectively. The parameter W_s is obtained from the data for low-energy implantation, in which nearly all positrons diffuse to and become trapped at the sample surface. W_s depends on the condition of the surface, and usually varies slightly from sample to sample. W_f is obtained from positron implantation at high energy, in which nearly all positrons annihilate in the defect-free bulk crystal beyond the depth of the ion-induced damage.

The fitting procedure is summarized in Fig. 1. A model defect distribution (based on TRIM, see below) is assumed. The fraction of positrons trapped in defects and at the surface is calculated for each positron energy. Then using Eq. (5) above, a W parameter is obtained and compared with the experimental results.

2. RBSC

Channeling and backscattering using light ions (typically 3-MeV He^+) is a well-established technique for measuring the depth distribution of defects created by ion implantation.[17] In contrast to positron annihilation, which is most sensitive to open volume defects (vacancies, voids, etc), the channeling technique measures the number of atoms that are displaced from their lattice sites (interstitial atoms, atoms in amorphous or disordered zones, etc.). In a simplified picture, channeled ions cannot backscatter from atoms at lattice sites, but may backscatter from displaced atoms. Nonchanneled (or dechanneled) ions will have a "random" backscattering probability from both lattice atoms and displaced atoms. Thus the normalized backscatter yield $\chi(z)$ (aligned yield divided by random yield) from depth z is given by

$$\chi(z)=[1-\chi_d(z)][N_d(z)/N]+\chi_d(z) . \tag{6}$$

In this equation $\chi_d(z)$ is the dechanneled component at depth z. $N_d(z)/N$ is the fraction of atoms displaced from their lattice sites. Some channeled ions will dechannel due to small angle deflections by displaced atoms, and thus the dechanneled fraction will increase as

$$\frac{d\chi_d}{dz}=\frac{\sigma_d N_d}{N}(1-\chi_d)\ . \tag{7}$$

At the surface no dechanneling has taken place, so the number of displaced atoms is given by

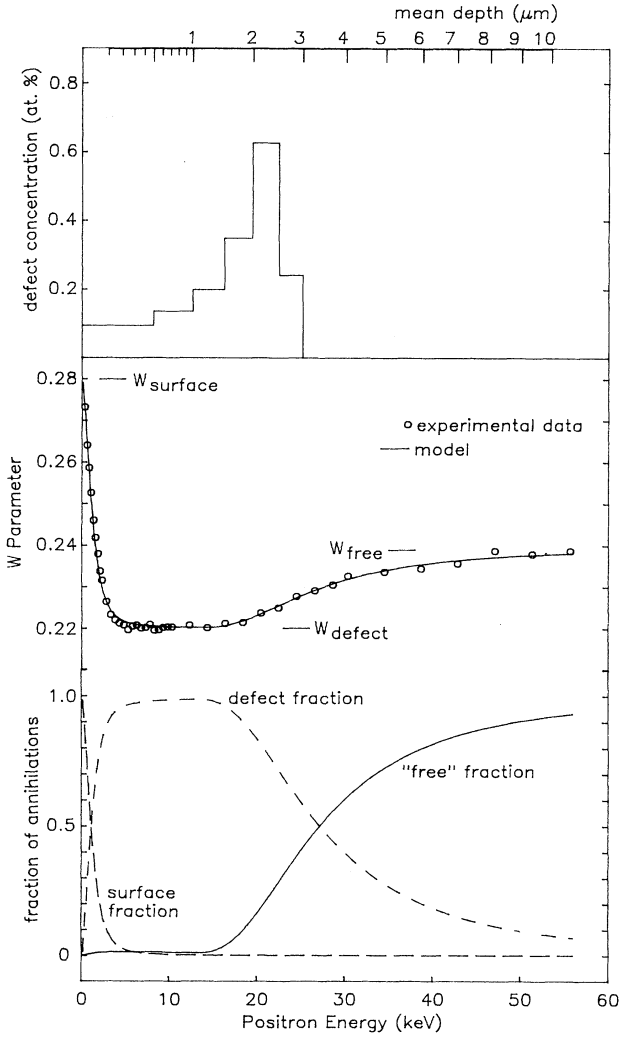

FIG. 1. The positron fitting procedure is illustrated, for the case of 10^{15} 3-MeV Si ions/cm^2. A defect distribution must first be assumed (top), in this case derived from the TRIM profile. The profile can be simulated with a few blocks of defects without loss of accuracy due to the smearing effects of the positron implantation profile and diffusion. The diffusion equation for positrons in the solid is then applied to determine the fraction of positrons annihilating in each of three states (bottom). The W parameter at each beam energy is then just a linear combination of these three states, producing the fit shown (solid line) in the middle figure.

$$N_d(0)=N\frac{\chi(0)-\chi_V(0)}{1-\chi_V(0)}\ , \tag{8}$$

where χ_V is the normalized yield from an unimplanted crystal. From the number $N_d(z)$ of displaced atoms we can calculate the increase of the dechanneled fraction at depth z and use this to successively determine the number of displaced atoms at larger depth.

This, together with the usual energy-to-depth conversion of an RBS spectrum, will provide us with a defect-depth profile. There is one unknown in these equations, the dechanneling cross section σ_d. This is chosen in such a way that the defect concentration at a depth much larger than the range of the ions is equal to zero.

3. *Infrared absorption (ir)*

Positron annihilation and channeling each provide information about a category of defects: open volume defects, and displaced atoms, respectively. In ion-implanted silicon an infrared absorption band centered at 1.8-μm wavelength is attributed to the divacancy.[18,19] Because the monovacancy becomes mobile in Si well below room temperature,[20] the divacancy is the simplest vacancy-type defect present. Moreover it has been shown that the infrared absorption technique can be calibrated so that an absolute areal density of divacancies can be determined.[21] A comparison between the number of vacancy-type defects observed by positron annihilation spectroscopy and the number of divacancies is then possible.

Samples for the infrared absorption experiments were polished on both sides and subsequently implanted from both sides in order to increase the signal strength. Optical transmission measurements were made at room temperature using a Nicolet Model 605X FTIR spectrometer.

4. *Computer simulations*

Useful information concerning the displacements due to ion bombardment can be obtained from computer simulations such as TRIM.[22] Results of TRIM calculations for the ion species and energies involved in this study are given in Fig. 2. For these calculations a displacement energy of 15 eV was assumed. These calculations give a good estimate of the number of atoms initially displaced by each incoming ion, and thus the depth distribution of vacancies. However, many of the defects initially formed will recombine or cluster, and such condensation processes are not included in the calculation. Also, the calculations assume an amorphous solid and thus do not simulate channeling effects of the implanted ions. For off-normal implantations this is an acceptable approximation for most purposes.

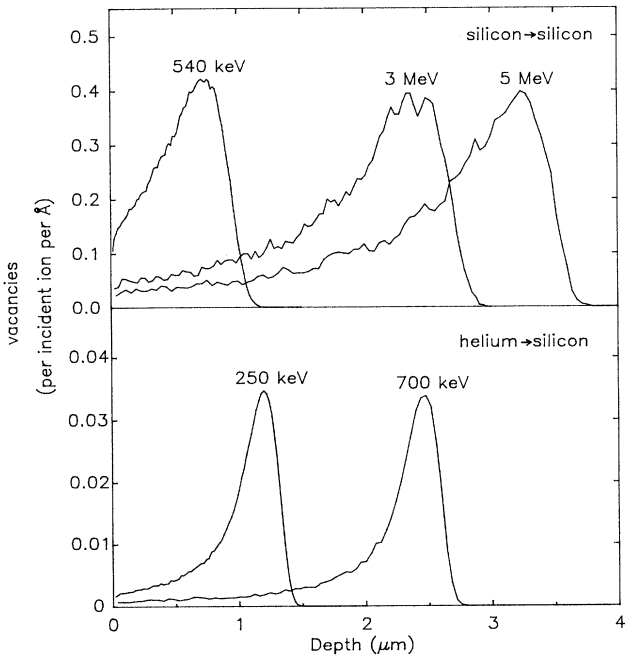

FIG. 2. The vacancy production as calculated using the TRIM code. The top panel shows the result for silicon implantation, and the lower one for helium. Note the difference in the vertical scales. The vacancy profiles for He^+ implantation, and to a lesser extent for Si^+ implantation are peaked near the end of range of the implanted ions.

III. RESULTS

A. Silicon implantation in silicon

1. Room-temperature results

It was only possible to determine damage profiles with the RBSC technique for fluences of 10^{14} cm^{-2} and above. In Fig. 3(a) we show the channeling spectra for samples implanted at a Si-ion energy of 540 keV, to fluences of 10^{14} and 10^{15} cm^{-2}. The calculated number of displaced atoms in the implanted layer was on the order of a few percent for the lower fluence and increased by only a factor of 2 for a tenfold increase in dose, i.e, saturation effects are becoming evident. The shapes of the extracted profiles [Fig. 3(b)] were in reasonable agreement with the damage profile calculated using the TRIM program (see Fig. 2). Results were also obtained for 3-MeV Si ion implantation to a fluence of 10^{15} cm^{-2} and are summarized in Table I.

Infrared absorption measurements performed on a sample implanted with 3-MeV energy Si ions to a fluence of 10^{14} ions cm^{-2} on back and front surfaces showed a divacancy concentration *per side* of 6.5×10^{15} cm^{-2}, well below the number of displaced atoms ($\sim10^{17}$ cm^{-2}) interpolated from the RBSC data.

With the positron annihilation technique, the development of the damage can be monitored down to much lower ion fluences than is possible by RBSC or infrared (ir) methods. Figure 4 shows the W parameter versus positron energy for silicon implanted with 540-keV Si^+ ions. For the unimplanted (virgin) sample the measured W parameter decreases slowly with positron energy until the "free" value W_f is reached. This is a consequence of the fact that with increasing energy fewer and fewer positrons will diffuse to and annihilate at the surface. For positron energies exceeding ~12 keV the W parameter is virtually constant, i.e., $W=W_f$. In a sample implanted to 10^{11} ions cm^{-2} we measured a small but significant change in the W parameter as a function of energy. Assuming the trapping rate $\nu=6\times10^{14}$ s^{-1} we obtained a defect production rate of ~180 per incident ion. This is much smaller than the number of vacancies per incident ion produced as calculated using the TRIM code (~1700 per ion). For increasing implantation dose, further decreases in the W parameter minimum were found, up to a dose of 10^{14} ions cm^{-2}. An implantation fluence of 10^{15} ions cm^{-2} gave an almost identical result to the 10^{14} ion cm^{-2} implantation. This means we were in the saturation regime, i.e., all positrons are trapped by defects.

The variation of damage range with Si ion implant energy is also reflected in the positron data. For implants of Si ions at energies of 0.54, 3.0, and 5.0 MeV the data

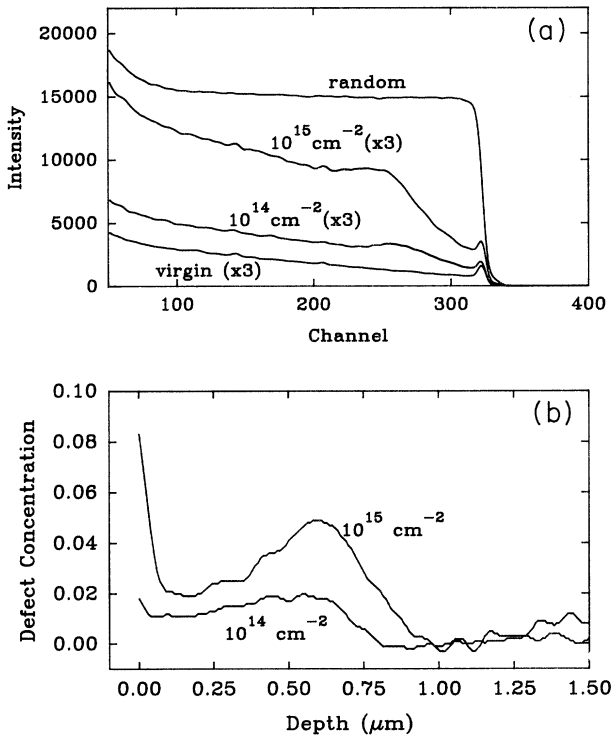

FIG. 3. The RBSC spectra of a sample implanted with 540-keV Si ions. 3-MeV He ions were used as an analyzing beam. The aligned spectra are enlarged three times for clarity. (b) shows the damage profiles as extracted from these data using the theory described in the text. The very sharp peak near the surface is probably a consequence of the somewhat different surface condition of the implanted and nonimplanted crystal.

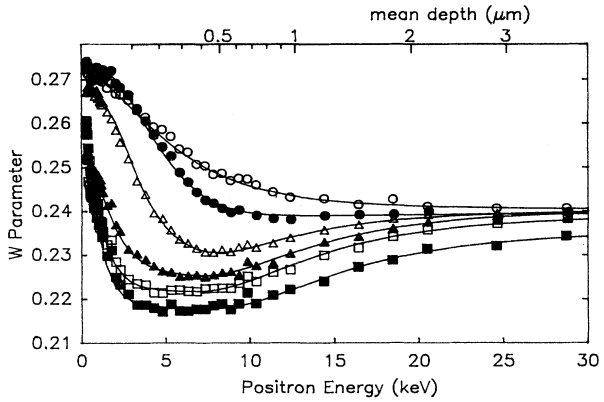

FIG. 4. The evolution of the W parameter as a function of fluence of 540-keV Si ions implanted. Unimplanted (○), and fluences/cm^2 of 10^{11} (●), 10^{12} (△), 10^{13} (▲), 10^{14} (□), and 10^{15} (■). Data for 10^{15} ions/cm^2 are displaced downwards by 0.005 for clarity. Solid lines show fits to the data. With increasing Si dose the W parameter around 5–10 keV decreases in value, as a consequence of an increase of the implantation damage. At doses higher than 10^{14} ions/cm^2 the W parameter does not decrease any more with increasing ion fluence because the positron trapping is saturated.

were well fitted by assuming the shapes (but not the absolute concentrations) of the defect profiles to be given by the TRIM calculations. (The authority for this rests on the accord between RBS data and TRIM calculations.) It should be noted that an acceptable fit to the 540-keV Si implant data can also be obtained, with similar W_d parameters, under the approximation that the defect concentration is constant from the surface to the maximum range (~ 0.8 μm). This approximation fails for higher-energy Si implantation conditions, as might be expected from inspection of the TRIM profiles in Fig. 2.

Figure 5 summarizes the relationship between defect concentrations (derived from positron measurements) and Si ion fluence. We assume for the two lowest Si ion fluences (10^{11} and 10^{12} ions cm^{-2}) that defect concentration will increase in proportion to ion fluence. Requiring that the ratio between the defect concentrations for these two fluences be a factor of 10 reduces by one the degree of freedom in the fitting procedure, and to obtain such a ratio it is *necessary* to use the defect parameter $W_d/W_f = 0.935 \pm 0.005$. This value can be associated with divacancies,[23] however, it is more likely in this case that W_d represents an average value for several defect types which may be present. As the ion fluence is increased, it is necessary to decrease W_d in order to fit the positron data. This change in W_d with ion fluence may

TABLE I. Summary of data. Defect concentrations (cm^{-2}) are shown as derived from positron annihilation, ir absorption (divacancies), RBS (number of displaced atoms), and TRIM. Numbers given for TRIM are obtained by multiplying the number of vacancies per incident ion resulting from the simulation by the ion fluence. Positron results marked by a * represent a lower limit on the defect concentration, and cannot be considered accurate due to the model of two competing defect types discussed in the text.

Energy (MeV)	Dose x (10^x/cm^2)	W_d/W_f	Defect concentration (cm^{-2}) Positron	ir (V-V)	RBSC	TRIM
			Si ions			
0.54	11	0.937	1.8×10^{13}			2.9×10^{14}
	12	0.937	1.8×10^{14}			2.9×10^{15}
	13	0.930	9.0×10^{14}			2.9×10^{16}
	14	0.923	3.0×10^{15}		5.5×10^{16}	2.9×10^{17}
	15	0.923	6.5×10^{15}		1.4×10^{17}	2.9×10^{18}
3.0	11	0.935	4.0×10^{13}			4.6×10^{14}
	12	0.935	2.9×10^{14}			4.6×10^{15}
	13	0.930	2.3×10^{15}			4.6×10^{16}
	14	0.920	1.1×10^{16}	6.5×10^{15}		4.6×10^{17}
	15	0.918	2.3×10^{16}		2.3×10^{17}	4.6×10^{18}
5.0	11	0.935	4.9×10^{13}			4.9×10^{14}
	12	0.935	4.9×10^{14}			4.9×10^{15}
	13	0.930	3.7×10^{15}			4.9×10^{16}
			He ions			
0.25	14	0.925	6.5×10^{14}*			1.6×10^{16}
0.5	16	0.913	2.7×10^{15}		7.7×10^{16}	
0.7	13	0.935	9.0×10^{13}			1.8×10^{15}
	14	0.935	9.0×10^{14}			1.8×10^{16}
	15	0.920	1.3×10^{15}*	1.3×10^{15}		1.8×10^{17}
	16	0.913	2.7×10^{15}*	2.6×10^{15}		1.8×10^{18}
4.0	14	0.935	1.8×10^{15}			2.3×10^{16}

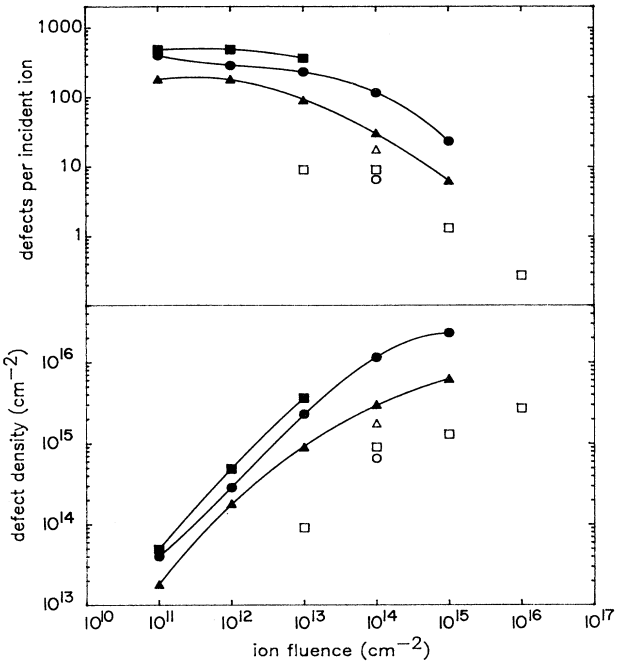

FIG. 5. The relationship between implantation dose and the number of defects as observed by positron spectroscopy. Silicon at 0.54 (▲), 3.0 (●), and 5.0 (■) MeV; helium at 0.25 (○), 0.7 (□), and 4.0 (△) MeV. Solid lines are a guide to the eye.

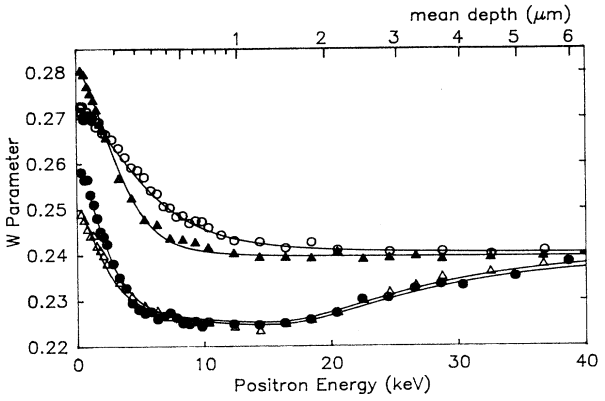

FIG. 6. Positron data for a sample implanted with 10^{13} 3-MeV Si ions/cm^2. The samples were annealed for 10 min in vacuum. The data are unchanged (except for small changes in the surface oxide) at 620 K, well above the divacancy annealing temperature. The main annealing occurs at temperatures in the 870–970 K range. Unimplanted (○), as implanted (●), annealed 620 K (△), annealed 970 K (▲).

be due to a change in the relative fractions of various defect types present, i.e., the fraction of large vacancy clusters (with smaller W_d values) increases with increasing damage density.

2. *Annealing*

RBSC measurements of a sample implanted to 10^{15} cm^{-2} with 0.54-MeV Si ions, then annealed for 10 min at 500 K, showed partial recovery of lattice order with a 50% reduction in the disorder signal. No further recovery was observed through isochronal annealing at 700 K. The disorder peak disappeared completely from the channeling spectrum after a 10-min anneal at 900 K, a temperature sufficient to activate the amorphous-to-crystalline transition.

By contrast, a 30-min anneal at 573 K of the 10^{14} cm^{-2} 3-MeV Si ion implant was sufficient to remove the 1.8-μm absorption peak from the infrared absorption spectrum, implying that the divacancies had annealed. A featureless absorption continuum at 2 μm and beyond indicated that optically active scattering centers remained in the sample.

The positron results from annealing of the 3-MeV Si implant, 10^{13} ions cm^{-2} are shown in Fig. 6. Annealing at 620 K, well above the divacancy annealing temperature of 560 K (Ref. 24) had only a small effect on the positron trapping (a change in the surface condition of the sample but no change in the bulk; in some cases the W parameters decreased marginally). While the conventional interpretation would be that the defects responsible for positron trapping had not changed, this is inconsistent with the ir evidence. If the disappearance of the divacancy absorption was to be attributed to a change in the divacancy charge state (assumed neutral), for example, it would be expected that the positron trapping would also change measurably. One possible explanation is that the vacancy distribution had altered in the direction of vacancy aggregates, i.e., multivacancy defects which are detectable by positron trapping but no longer optically active at a 1.8-μm wavelength.

Annealing to 970 K resulted in recovery of the crystal to near preimplant quality, with a defect concentration $<1\%$ of that prior to annealing. The nature of the remaining defects, stable to high temperatures, is not known.

B. Helium implantation in silicon

1. *Room-temperature results*

RBSC data were obtained for a sample implanted with 10^{16} He ions cm^{-2} at an energy of 500 keV. The difference between the implanted and unimplanted samples was small, significant only near the end-of-range of the 500-keV He ions. The peaked damage profile derived from these data, and the lower level of damage introduced by He ion implantation compared to Si ion implantation, are reflected in the TRIM calculations shown in Fig. 2.

Infrared measurements of a silicon sample implanted from each side with 1.0×10^{16} He ions cm^{-2} at 700 keV showed the divacancy concentration to be 2.55×10^{15} cm^{-2} per side.

Positron data were obtained for 700-keV He implantation doses of 10^{13}, 10^{14}, 10^{15}, and 10^{16} ions cm^{-2}. Derived defect concentrations are given in Table I. The defect concentration increases in proportion to the He ion fluence between 10^{13} and 10^{14} cm^{-2}, reminiscent of the silicon ion data. The data for the 10^{15} and 10^{16} ions cm^{-2}

doses were very similar. This is due to the same saturation effect discussed previously for Si ion irradiation, i.e., in the energy range ~6–10 keV, nearly all positrons annihilate from a defect-trapped state, and the addition of more defects has little effect on the measured γ-ray line shape. The saturation value for W in this case is the same as that observed for Si ions (Fig. 4), suggesting that differences in the damage caused by high-fluence light- and heavy-ion irradiations cannot be distinguished by positron spectroscopy alone. The defect model used to fit the data for the 10^{13} and 10^{14} ions cm^{-2} cases was based on the shape of the vacancy profile produced by the TRIM simulation program, and the absolute defect concentration was varied until a good fit was obtained. However, it was found that for the higher dose 700-keV helium implants (10^{15} and 10^{16} ions/cm^2), the W vs. E curve could not be fitted with a defect profile shape based on TRIM calculations, or, equivalently, on RBSC data. In order to fit the positron data it was necessary to assume a shallower defect profile, with the majority of the defects at a depth of less than 1 μm. The range predicted for the implanted ions is ~2.5 μm, and the majority of the damage is expected to be near the end of range.

Similar disagreement has been reported by others who have used positron methods to study implantation damage in silicon by 12-MeV Si,[25] 100-keV P,[26] 35-, 60-, and 100-keV H,[27] and 80-keV B.[28]

Positron data were obtained for samples implanted at energies of 250 keV, 700 keV (as discussed above), and 4 MeV at a fluence of 10^{14} He ions/cm^2. The range of the damage increases with He ion energy. The positron data were fitted using the TRIM profile for the vacancy distribution. (In the 4-MeV case, the ion range, ~17 μm, is greater than the maximum attainable positron range, ~12 μm at 60 keV.) For the 250-keV case it was found that the extracted damage profile was again shallower than predicted by TRIM, as it was for the higher-dose implants at 700 keV.

By increasing the energy of the implanted He ions from 250 keV to 4 MeV we had changed the nuclear stopping close to the surface by about a factor of 10 but the electronic stopping by not more than a factor of 2. The large difference in the observed defect density close to the surface between the 250-keV and 4-MeV implantations suggests very strongly that the damage scales with nuclear, rather than electronic, stopping, in accordance with the generally accepted view of damage production in Si.[29]

2. *Annealing*

Annealing of the He-implanted silicon at 570 K for 1 h removed the majority of damage, as shown by the positron data in Fig. 7 for the case of 10^{16} cm^{-2} 500-keV He ions. This temperature is close to the reported divacancy annealing temperature of 560 K.[24] Annealing at this temperature also removed the 1.8-μm infrared absorption. Monitoring the W parameter at a positron energy of 12 keV (mean depth ~0.9 μm) during an *in-situ* anneal showed no change in the sample below ~560 K. We conclude that the defect responsible from the majority of

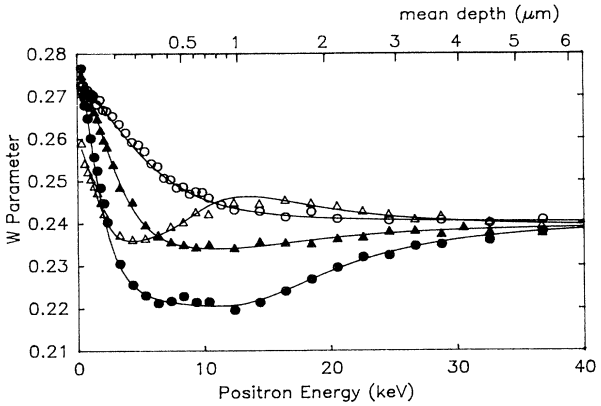

FIG. 7. The annealing of the 500-keV He implanted sample. In contrast to the case of Si ion implantation the damage anneals near 570 K, the temperature range at which the divacancy becomes mobile. Unimplanted (○), as implanted (●), annealed 570 K (△), annealed 970 K (▲).

positron trapping in these samples below this temperature was the divacancy. In the case of the higher doses (10^{15} and 10^{16} He ions/cm^2) however, it was noted that a second type of defect, with $W_d/W_f > 1$, appeared after annealing. We speculate that this is caused by a helium-related defect, since it appears to be at approximately the end of range of the implanted ions, ~2.5 μm (positron energy ~20 keV). This suggests that the discrepancy between depths of damage obtained from the positron measurements and other techniques may be caused by a superposition of two defect types with opposing effects on the γ-ray line shape. Why this is not seen for all cases of He implantation is not clear but may be related to the concentration of He in the sample, since it was observed for the two highest doses at 700 keV, and for the 10^{14} cm^{-2} 250-keV sample, in which the shorter ion range results in an increased He ion concentration.

IV. DISCUSSION

A. Positron trapping rates

Recent positron lifetime measurements gave positron trapping rates of $\nu = 0.5$ to 1.0×10^{15} s^{-1} for neutral divacancies, 1.8 to 3.5×10^{15} s^{-1} for negative divacancies, and 3.5 to 7.0×10^{15} s^{-1} for doubly negative divacancies.[30] In the p-type wafers used for this study, and for defect concentrations high enough to drive the local material intrinsic—which is approached under most of our Si ion implant conditions—we expect the majority of divacancies to be neutral.[28] For the sample implanted with 10^{14} 3-MeV Si ions cm^{-2}, we measured 1.1×10^{16} defects cm^{-2} while infrared absorption indicates there were 6.5×10^{15} divacancies cm^{-2}. We can adjust the rate ν to give exact agreement between these; then $\nu = 1.0\times10^{15}$ s^{-1}, consistent with Mascher, Dannefaer, and Kerr[30] to within the experimental uncertainty. This, however, does not take into consideration that defects other than the divacancy, or a mixture of divacancy charge states, may be trapping positrons. The helium implantation data cannot

be used with confidence for such a comparison because of the possibility of two competing defect types as discussed above.

This would indicate that the dominant positron trapping species is the divacancy. To reconcile this with the absence of an annealing stage at the divacancy annealing temperature for the Si implants, we speculate that upon annealing the divacancies agglomerate into larger vacancy clusters, with the product νC (concentration times positron trapping rate) remaining roughly constant. This would explain the apparent disagreement between the positron measurements and other techniques for annealed samples.

B. Defect production rates

In the limit of low fluences, the number of vacancies per incident ion measured by positrons is 0.1–0.2 of that calculated by TRIM. This suggests that ~85% of the Frenkel pairs produced annihilate by recombination.

C. Dose dependence

Because of interactions between damage cascades, the defect concentration increases less than linearly with ion fluence for fluences above $\sim 10^{12}$ cm^{-2} for Si ions and $\sim 10^{14}$ cm^{-2} for He ions. It is not possible to fit the positron data if one assumes that the number of defects and ion dose increase proportionally beyond 10^{12} ions cm^{-2} for Si and 10^{14} ions cm^{-2} for He.

D. Energy dependence

The positron data for Si implantation and the low-dose He implantations could be well fitted assuming the shape of the defect distribution as obtained from TRIM calculations and from RBSC. For the high-dose He ion implanted samples the positron results disagree with both TRIM and RBSC results. The positron results indicate a shallower damage depth than that established by these other techniques. This may be an indication of the formation of a He-related defect at larger depth, which influences the W parameter in the opposite direction. The amount of damage observed for the He implants is proportional in all cases to the nuclear stopping of the implanted ion.

E. Temperature dependence

There is a clear difference in the annealing behavior of the He and Si implanted samples. In the case of Si implantation, the level of the damage measured by positrons remains roughly constant up to temperatures at which amorphous Si recrystallizes (~870 K). In the case of He irradiation, the damage seems to anneal out at (or a little above) the temperature at which the divacancy becomes mobile. From the infrared measurements we know that in both cases a considerable number of divacancies are present. In positron lifetime spectroscopy experiments, at the temperature at which divacancies became mobile, an increase in the lifetime of the trapped positrons was observed (larger vacancy clusters grow by agglomeration of more than one divacancy) whereas the trapped fraction decreased (fewer of these larger clusters).[31,32] A similar phenomenon may be occurring in our samples, but it is not trivial to predict how the cluster size will influence the γ-ray line shape in Doppler-broadening measurements. Besides agglomeration, the divacancies can also be trapped at an interstitial cluster and annihilate in this way. It may be that a different ratio of the recombination and agglomeration processes in the Si and He cases causes the qualitatively different behavior. However, this question is far from settled.

ACKNOWLEDGMENTS

The authors would like to thank H. J. Stein for performing the infrared absorption measurements and G. Mulligan for the operation of the accelerator. We are grateful to J. C. McCallum for stimulating discussions. This research was financed in part by the Ontario Centre for Materials Research and the National Science and Engineering Research Council of Canada.

[1] J. W. Mayer, L. Eriksson, S. T. Picraux, and J. A. Davies, Can. J. Phys. **46**, 663 (1968).

[2] L. M. Howe and M. H. Rainville, Nucl. Instrum. Methods **B19/20**, 61 (1987).

[3] R. G. Elliman, J. Linnros, and W. L. Brown, in *Fundamentals of Beam-Solid Interactions and Transient Thermal Processing,* edited by, M. J. Aziz, L. E. Rehn, and B. Stritzker, MRS Symposia Proceedings No. 100 (Materials Research Society, Pittsburgh, 1988), p. 363.

[4] F. Priolo, C. Spinella, and E. Rimini, Phys. Rev. B **41**, 5235 (1990).

[5] J. W. Corbett, J. P. Karins, and T. Y. Tan, Nucl. Instrum. Methods **182/183**, 457 (1981).

[6] H. J. Stein, F. L. Vook, D. K. Brice, J. A. Borders, and S. T. Picraux, Radiat. Eff. **6**, 19 (1970).

[7] O. W. Holland, S. J. Pennycook, and G. L. Albert, Appl. Phys. Lett. **55**, 2503 (1989).

[8] P. J. Schultz and K. G. Lynn, Rev. Mod. Phys. **60**, 701 (1988).

[9] E. Tandberg, P. J. Schultz, G. C. Aers, and T. E. Jackman, Can. J. Phys. **67**, 275 (1989).

[10] I. V. Mitchell, P. J. Simpson, P. J. Schultz, M. Vos, U. Akano, and C. Wu, in *Positron Beams for Solids and Surfaces,* edited by P. J. Schultz, G. R. Massoumi, and P. J. Simpson (AIP, New York, 1990), p. 121.

[11] It now appears that changes in temperature of this magnitude may be sufficient to alter significantly the type of damage remaining after annealing; P. J. Schultz, C. Jagadish, M. C. Ridgeway, R. G. Elliman, and J. S. Williams, Phys. Rev. B **44**, 9118 (1991).

[12] P. J. Schultz, Nucl. Instrum. Methods **B30**, 94 (1988).

[13] S. Valkealahti and R. M. Nieminen, Appl. Phys. A **35**, 51 (1984).

[14]P. J. Schultz, E. Tandberg, K. G. Lynn, B. Neilsen, T. E. Jackman, M. W. Denhoff, and G. C. Aers, Phys. Rev. Lett. **61**, 187 (1988).

[15]We assume the predominant defect type is the divacancy and thus use as an approximation twice the monovacancy trapping rate (3×10^{14} s^{-1}) given by S. Dannafaer, Phys. Status Solidi A **102**, 481 (1987).

[16]G. C. Aers, in *Positron Beams for Solids and Surfaces* (Ref. 10), p. 162.

[17]L. C. Feldman, J. W. Mayer, and S. T. Picraux, *Materials Analysis by Ion Channeling* (Academic, New York, 1982).

[18]H. J. Stein, F. L. Vook, and J. A. Borders, Appl. Phys. Lett. **14**, 328 (1969).

[19]H. J. Stein and W. Beezold, Appl. Phys. Lett. **17**, 442 (1970).

[20]W. Fuhs, U. Holzhauer, and F. W. Richter, Appl. Phys. **22**, 415 (1980).

[21]L. J. Cheng and J. Lori, Phys. Rev. **171**, 856 (1968).

[22]J. P. Biersack and L. G. Haggmark, Nucl. Instrum. Methods **174**, 257 (1980).

[23]Fitting S parameters [a related measure of γ-ray line width (Refs. 8 and 9)] extracted from the same experimental data, we find $S_d=1.035\pm0.005$, in agreement with values previously identified with divacancies, e.g., $S_d=1.034$ (Ref. 27).

[24]G. D. Watkins and J. W. Corbett, Phys. Rev. **138**, A543 (1965).

[25]A. Vehanen, in *Positron Annihilation,* edited by L. Dorikens-Vanpraet, M. Dorikens, and D. Segers (World Scientific, Singapore, 1989), p. 39.

[26]P. Hautojärvi, P. Huttunen, J. Mäkinen, E. Punkka, and A. Vehanen, in *Defects in Electronic Materials,* edited by M. Stavola, S. J. Pearton, and G. Davies, MRS Symposia Proceedings No. 104 (Materials Research Society, Pittsburgh, 1988), p. 105.

[27]J. Keinonen, M. Hautala, E. Rauhala, V. Karttunen, A. Kuronen, J. Raisn, J. Lahtinen, A. Vehanen, E. Punkka, and P. Hautojärvi, Phys. Rev. B **37**, 8269 (1988).

[28]A. Uedono, S. Tanigawa, J. Suguira, and M. Ogasawara, in *Positron Annihilation,* edited by L. Dorikens-Vanpraet, M. Dorikens, and D. Segers (World Scientific, Singapore, 1989), p. 690.

[29]J. A. Davies, in *Ion Implantation and Beam Processing,* edited by J. S. Williams and J. M. Poate (Academic, New York, 1984), p. 81.

[30]P. Mascher, S. Dannefaer, and D. Kerr, Phys. Rev. B **40**, 11 764 (1989).

[31]S. Dannefaer, G. W. Dean, D. P. Kerr, and B. G. Hogg, Phys. Rev. B **14**, 2709 (1976).

[32]P. Mascher, S. Dannefaer, and D. Kerr, Mater. Sci. Forum. **38-41**, 1157 (1989).